Small Angle Scattering for Pharmaceutical Applications: From Drugs to Drug Delivery Systems

15

Aaron Alford, Veronika Kozlovskaya, and Eugenia Kharlampieva

Abstract

The sub-nanometer scale provided by small angle neutron and X-ray scattering is of special importance to pharmaceutical and biomedical investigators. As drug delivery devices become more functionalized and continue decreasing in size, the ability to elucidate details on size scales smaller than those available from optical techniques becomes extremely pertinent. Information gathered from small angle scattering therefore aids the endeavor of optimizing pharmaceutical efficacy at its most fundamental level. This chapter will provide some relevant examples of drug carrier technology and how small angle scattering (SAS) can be used to solve their mysteries. An emphasis on common first-step data treatments is provided which should help clarify the contents of scattering data to new researchers. Specific examples of pharmaceutically relevant research on novel systems and the role SAS plays in these studies will be discussed. This chapter provides an overview of the current applications of SAS in drug research and some practical considerations for selecting scattering techniques.

Keywords

Small angle scattering • Pharmaceutical • Structural characterization • Delivery vehicles • Nanoparticles • Micelles • Vesicles • Multilayer capsules

15.1 SAS Data Analysis

There are many methods of modeling and interpreting SAS data. Figure 15.1 shows an overview of the most common techniques used *ab initio* to interpret the data gathered in structural studies. Starting from the common Porod

A. Alford • V. Kozlovskaya • E. Kharlampieva (✉)
Department of Chemistry, University of Alabama at Birmingham, 901 14th Street South, CHEM 272, Birmingham, AL 35294, USA
e-mail: ekharlam@uab.edu

B. Chaudhuri et al. (eds.), *Biological Small Angle Scattering: Techniques, Strategies and Tips*, Advances in Experimental Medicine and Biology 1009, DOI 10.1007/978-981-10-6038-0_15

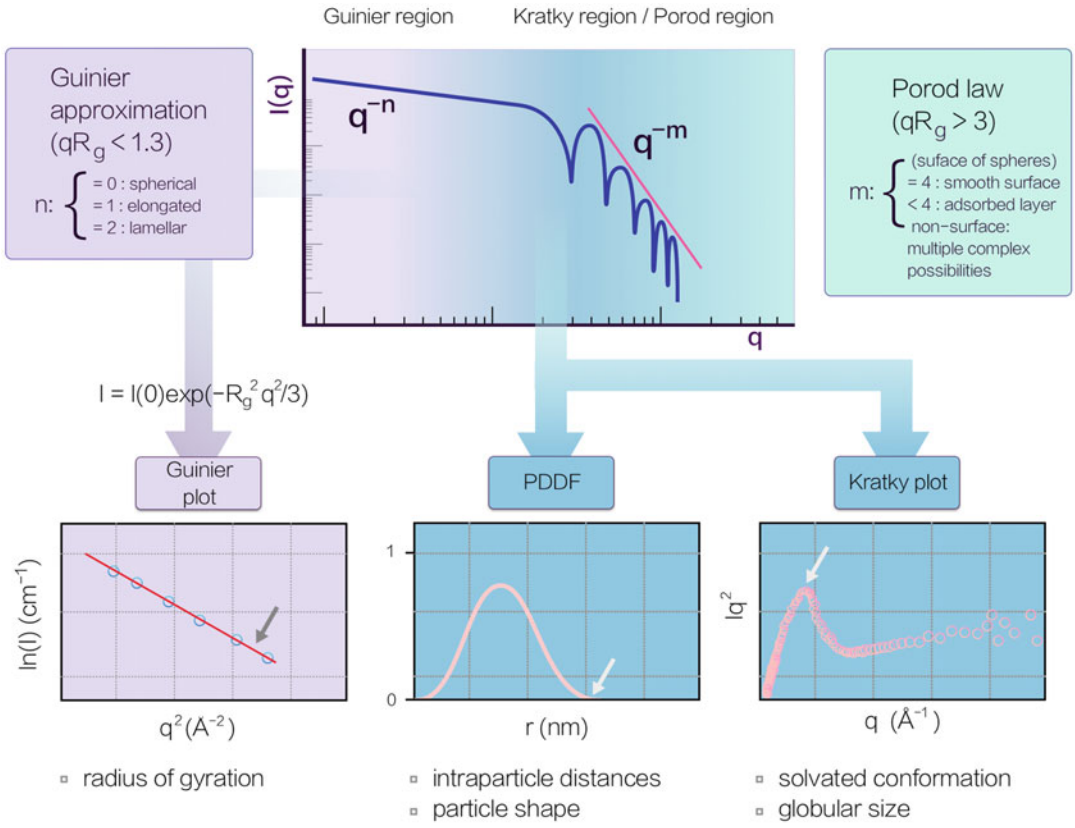

Fig. 15.1 Different regimes in scattering curves with the relevant structural information defined for each method of analysis

(log-log) plot most often encountered from reduced data, the first of the model-free analyses is the Guinier approximation used to estimate the radius of gyration, R_g, and generalized particle form. This is a common first step for data on drug delivery carriers in the 50–200 nm size range. The Guinier range is the region of q such that $qR_g<1.3$ and the q^n dependency of the form factor in this range of the log-log plot describes in general the morphology of the scattering body with n = 0, 1, and 2 representing globular (spherical), rod-like, and lamellar (flat) morphologies, respectively (Schnablegger and Singh 2013). It is important to note that several assumptions of ideality must be taken in this analysis. First, since the intensity of scattering I as a function of the scattering vector q is a product of two factors, following Eq. 15.1,

$$I(q) = P(q)\,S(q) \tag{15.1}$$

where $P(q)$ and $S(q)$ are the form and structure factors, respectively, sufficient dilution must be achieved such that the form factor can be analyzed independently of the contribution from the structure factor. The reason for this is that the scattering contribution from the structure factor due to interparticle interactions and arrangement in diluted systems is minimal such that it tends to approach unity and the intensity therefore becomes equal to the form factor (Guinier and Fournet 1955). Guinier's approximation is made in reference to the form factor with sufficient dilution being assumed. This is a particularly important consideration for drug delivery carriers that exist as insoluble suspensions. Secondly, monodispersity of the particles is a requirement for the most

accurate approximation, as small polydispersities affect the slope of the scattering curve significantly at very small q. With these assumptions fulfilled, an expansion of Guinier's original theory (Glatter and Kratky 1982) takes the form of

$$I = I(0)\exp\left(\frac{-R_g^2 q^2}{3}\right) \qquad (15.2)$$

where I is the scattering intensity. Plotting $\ln(I)$ vs q^2 therefore gives the R_g from the slope of the fit line once it is extrapolated to the intercept $I(0)$.

The next region in the log-log plot encompasses the intermediate values of q between the Guinier range and Porod range ($qR_g > 3$). Indirect Fourier Transform (IFT) and Kratky analyses both produce useful plots from this region with the IFT providing a Pair Distance Distribution Function (PDDF). The PDDF represents a distribution of the intraparticle distances elucidated by the scattered radiation. The shapes produced by this plot are characteristic of specific form factors and again present model-free approximations as well as another representation of the particle size with the largest intraparticle distance(s) being the distance from one terminal edge of the particle to another (Schnablegger and Singh 2013). This distance is found at the end of the rightmost shoulder for spherical particles and other shapes have multiple points at which critical dimensions are represented. Figure 15.2 shows a representation of various PDDF plot shapes with their corresponding morphologies and size indications.

Flowing from the same region of q is the Kratky plot of Iq^2 vs q which gives insight into the conformation of polymers in solution from their mid to high q scattering. At the higher part of this q range, Gaussian coiled polymers result in scattering that follows $1/q^2$ behavior and so tend to produce curves that level out in the Kratky plot. Deviation from this line-shape indicates non-Gaussian conformations, the source of which is usually interpreted by the researcher based on the sample composition. The shape of the curve in a Kratky plot can therefore be used to distinguish between stretched Gaussian coil polymers or non-ideal conformations due to attractive/repulsive forces

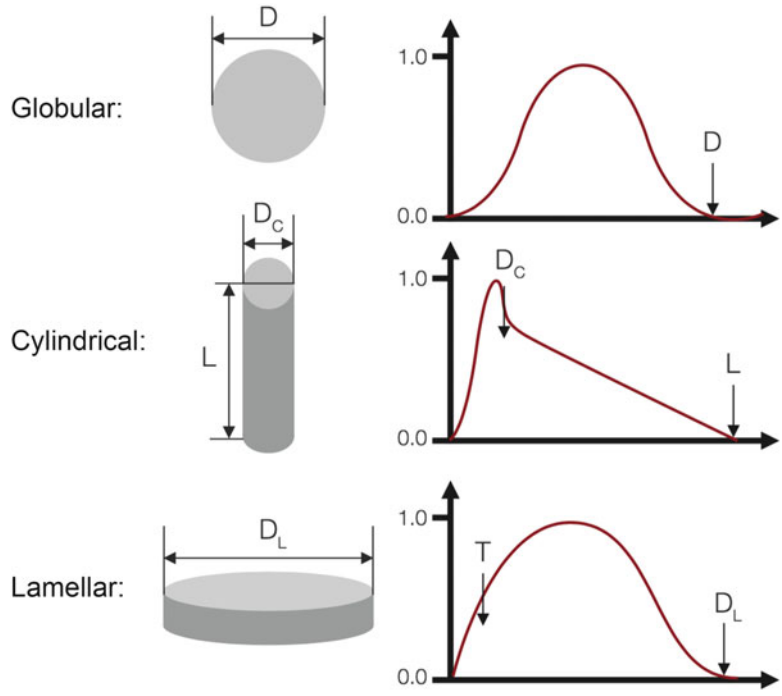

Fig. 15.2 Determination of critical dimension and shape from PDDF plots (Schnablegger and Singh 2013) (Reprinted with permission from Anton Paar GmbH)

that result in excluded volume (Hammouda 2016). For drug delivery applications involving self-assembled systems, polymer conformation can be an important piece of information.

Deeper application of this analysis in drug delivery vehicle structural research will be clear when the following is considered: if Gaussian chains result in a curve with a slow rise that levels into a plateau, self-associative forces that lead to precipitation and the formation of nano-objects are characterized by a peak in the initial region of the Kratky plot. The position of this peak is inversely proportional to the R_g (Filippov et al. 2012). Especially in systems of complex multi-component structure, such as drug-conjugated copolymers, this analysis provides detail of the solvated or structural morphology that can be focused using contrast variation techniques.

The Kratky and PDDF analysis techniques were used to probe constructs of 2-hydroxypropylmethacrylamide (HPMA) copolymers containing cholesterol moieties and doxorubicin in elegant characterizations that revealed the conformation of polymers within the nanoparticle structures as rounded cylinders (Filippov et al. 2012, 2013). Kratky analysis and cross-sectional PDDF in this case showed that the nanoparticle structure changed from Gaussian coiled coronas to more compact objects with higher excluded volume as a function of the concentration of cholesterol moieties (0–3.0 mol%) in the chain (Filippov et al. 2012). The power of modeling software and the true richness contained within scattering data can be seen in Fig. 15.3 (Kratky and PDDF) from the same study in which computational analysis

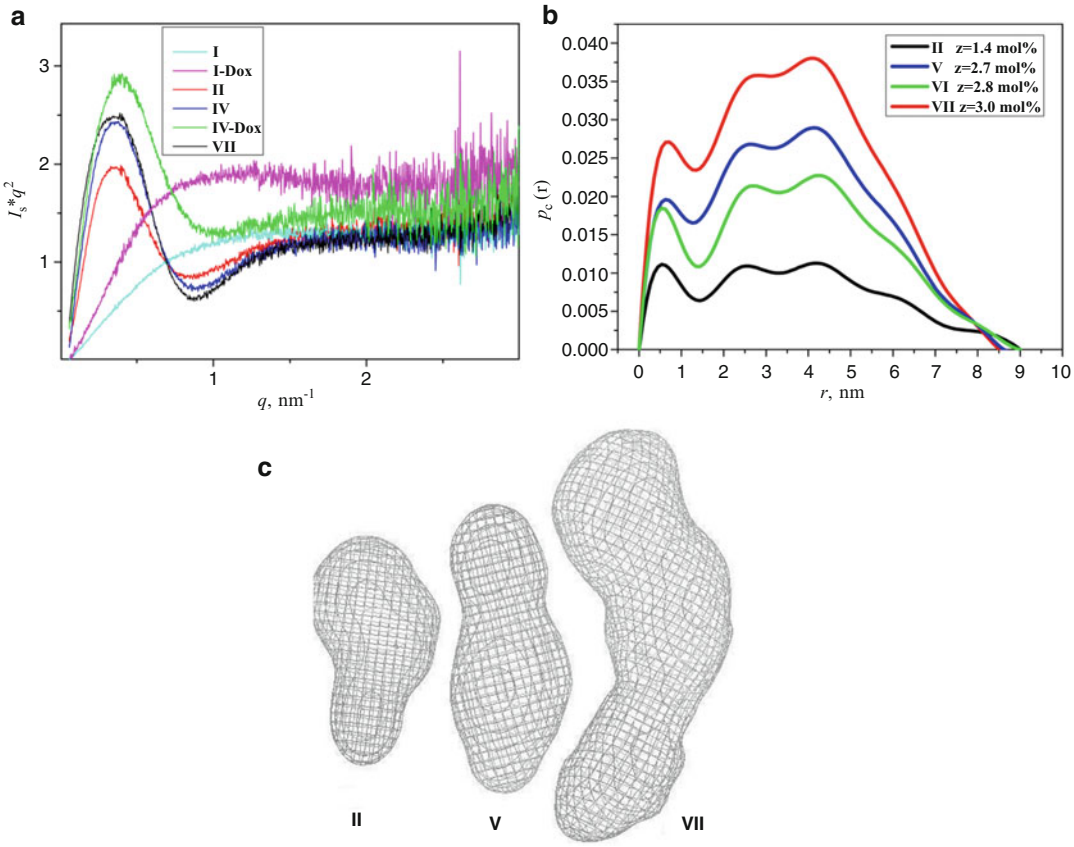

Fig. 15.3 Kratky (**a**) and cross-sectional PDDF (**b**) plots showing morphology and cross-sectional distances of conjugates used to compute the hypothetical structure (**c**) (Reprinted with permission from Filippov et al. 2012, copyright American Chemical Society)

yielded hypothetical shapes of the nanoparticles from cross-sectional PDDF as ellipsoids with lengths of 12.1 nm and widths of 4.6 nm.

After the Guinier and Kratky analyses, the final type of model-free data to be obtained comes from the region of the standard scattering plot known as the Porod range where $qR_g > 3$. The slope of the q^{-m} dependency in this region is dependent on the surface per volume according to Porod's law and the value of m can speak about the physical properties of the surface scattered at large angles. An m value of 4 at high q is indicative of a smooth surface for spherical objects while $2 < m < 4$ represents scattering due to a rougher adsorbed layer (Estrela-Lopis et al. 2009). Extensive multi-slope plots, their q^{-m} laws, and their shape implications can be found in the works of Boualem Hammouda (2010a, b, 2016). Plots built from combined concepts such as Kratky-Porod reveal even greater detail from advanced methods and will be discussed later in the chapter.

Outside of these model-free techniques there are a multitude of model-intensive approaches often used within analysis environments such as SASview, PRIMUS, and others that can fit scattering curves to relevant physical parameters. However, since scattering curves are not fingerprints, the models must be informed to avoid unreasonable parameter definitions. This is an important point for characterization of drug delivery vehicles and is one of the predominate reasons that supplementary characterizations are often performed alongside SAS. The fewer parameters that are left to float during model fitting routines, the more accurate the remaining parameters can describe the scattering curve and the better the picture that can be obtained with SAS. Modeled approaches are often used if the shape or form of the particle is known *a priori*; therefore data fitting approaches should start from model-free analysis before moving into precise characterization with fitting models. The workings of model fitting are not discussed in detail due to their highly specific and customizable nature. However, model analysis is still present in nearly every SAS study, as the parameters are highly relevant especially in terms of the properties of drug delivery devices. This will be seen in the following sections.

15.2 Structural Characteristics of Drugs and Drug Delivery Vehicles

15.2.1 Delivery Vehicles

15.2.1.1 Nanoparticles

Nanoparticles can be defined as nanometer-sized clusters of atoms or molecules. Nanoparticles come in many shapes and have been gaining popularity as drug delivery vehicles (Urbina et al. 2008; Mattingly et al. 2015). Owing to their small size (1–100 nm), tunable composition, and potential inclusion of metals to imbue them with fluorescent/IR/magnetic sensitivities they often have unique properties in terms of cellular uptake, bio-distribution, and reactivity to stimuli (Remant Bahadur et al. 2012). These properties also make them common candidates for SAS studies because, while other techniques can give size information, they fall short in characterizing the internal structures and inter-particle interactions that make nanoparticles unique and useful for drug delivery.

15.2.1.2 Micelles

Micelles are single or dual-component nanometer-sized formations of amphiphilic molecules dispersed in a solvent, often water, that generally have spherical morphology but are not strictly limited to spheres (Biggs et al. 2007). Micelles have a core-corona architecture featuring hydrophobic cores and hydrophilic coronas when used in aqueous environments. Micelles often self-assemble in water to stabilize the interactions of the two portions of the molecule with the solvent, with reverse micelles possible in the case of hydrophobic solvents (Nunes and Car 2013; Correa et al. 2012). Block copolymers are widely utilized as micelle forming delivery devices and often include PEG paired with a less hydrophilic polymer such as poly(lactic acid) or polystyrene (Cho et al. 2006; Bae et al. 2009). SAS studies

with micelles often utilize contrast variation techniques and/or selective deuteration of components to isolate them from the overall scattering in efforts to characterize their structural components (Almgren et al. 2007; Naruse et al. 2009; Smith et al. 2014).

15.2.1.3 Vesicles

Polymeric vesicles are multi-component nanometer- or micrometer-sized assemblies of amphiphilic molecules dispersed in a solvent. Vesicles are similar to micelles in terms of their components, but in contrast, form hollow spherical or worm-shaped structures with solvent trapped in the inner cavity and a hydrophobic bilayer between the core cavity and hydrophilic corona (Srinivas et al. 2013; Sauer and Meier 2004). Vesicle applications within drug delivery are often similar to those of micelles, with some systems able to switch from one morphology to the other in response to stimuli (Lagzi et al. 2010).

15.2.1.4 Multilayer Capsules

Multilayer capsules are nanometer to micron-sized polymer constructs made of ionic, hydrogen-bonded, or covalently bonded layers of polymers or other constituents (Kharlampieva et al. 2009; Kozlovskaya et al. 2009, 2012a, b; Erel-Unal and Sukhishvili 2008). Hollow hydrogel microcapsules are formed by layer-by-layer (LbL) assembly of polyelectrolytes on sacrificial particulate templates, followed by chemical cross-linking of the assembled polyelectrolyte multilayer and template dissolution (Sukhorukov and Möhwald 2007; Wang et al. 2008; Skirtach et al. 2011). LbL technology offers unique opportunities to fabricate capsules of any size, geometry, composition and thickness controlled at the nanoscale (Lvov et al. 1993; Decher 2002; Kharlampieva and Sukhishvili 2006; Lutkenhaus and Hammond 2007; Hammond 2011; Mjahed et al. 2008; Tang et al. 2006). The technique can synthetically recreate shapes and easily impart a desired elasticity and responsiveness to the thin capsule wall (Elsner et al. 2006; Lisunova et al. 2011). The capsule's wall can be easily functionalized, with an internal cavity which can be used for loading functional compounds. Unlike other competing delivery systems such as nanoparticles, liposomes, dendrimers, and block copolymer vesicles and micelles, nanothin capsules have a high loading capacity and can deliver cargo on demand in response to a stimulus (Donath et al. 1998; Caruso et al. 1998; Becker et al. 2010; Matsusaki and Akashi 2009; Tong and Gao 2008). Because of their templated construction and multilayer or hydrogel architecture, capsules have greater structural stability compared to vesicles and micelles (Liu et al. 2014; Kozlovskaya et al. 2012a, b). Their core-shell structure and potential for selective deuteration both make polymer capsules interesting candidates for SAS studies where characterization of the shell thickness, capsule morphology, or cargo in the cavity can only be determined through precise methods.

While efforts are being directed toward making drugs more selective by their structural design, at least as many efforts are aimed at developing smart carriers that can chaperone drugs that have high efficacy but limited selectivity to their intended target in the body, thus minimizing collateral damage from rogue drug molecules by releasing them in a controlled manner *via* biologically relevant triggers such as pH, temperature, and presence of cellular peptides (Xue et al. 2015; Liu et al. 2015; Kozlovskaya et al. 2014).

The structures of these drug carriers range from micelles and vesicles between 5 and 200 nm in diameter (Fig. 15.4) to larger constructs including capsules and gel particles in the 1–10 μm range and, although they function according to their intended purpose, researchers are often left hypothesizing about *exactly* what happens during response to the stimulus, release of the drugs, or sometimes even exactly what size or shape the carriers are. Due to their extremely diminutive nature, characterizing the shape and structure of a drug carrier such as a nanoparticle can be challenging without advanced techniques (Mariani et al. 2016). SANS and SAXS are among these techniques: they can probe the structures of these innovative materials to evaluate carrier's shape and size, interior and exterior

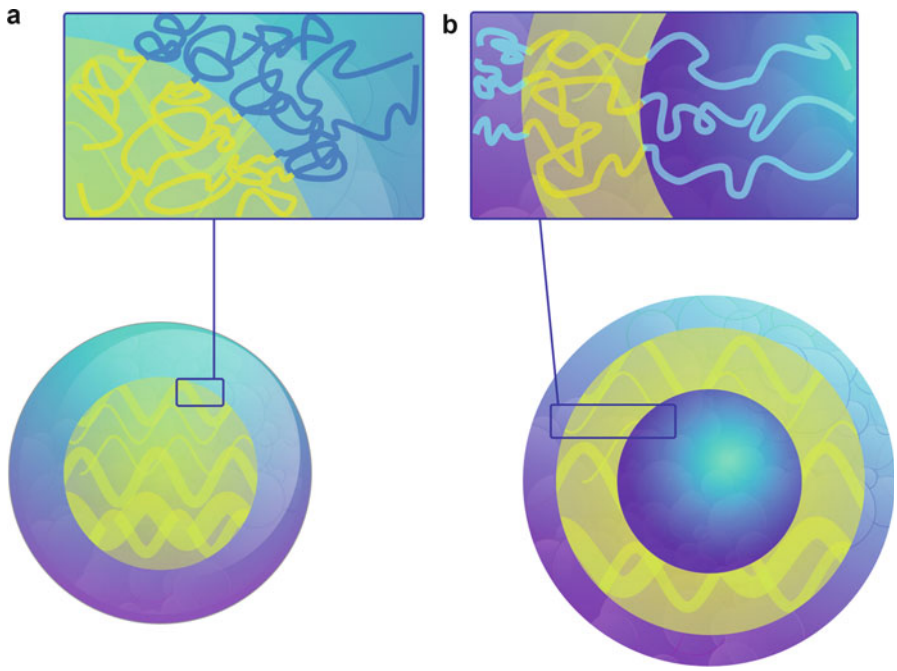

Fig. 15.4 Schematic of the internal structure of micelles (**a**) and vesicles (**b**) where hydrophobic portions of the molecule are shown as *yellow* and the hydrophilic portions are *colored blue*

dimensions, layer spacing and stratification, interparticle spacing and interaction behaviors, and dynamic assembly with the proper experimental design and material construction (Lu et al. 2016; Fong et al. 2010; Yin et al. 2016). For instance, consider an amphiphilic molecule or polymer in D_2O (Fig. 15.4). Since the scattering length density (SLD) values for the protium and deuterium isotopes of hydrogen lie on opposite sides of a spectrum of values, hydrogen-containing molecules in D_2O will have an SLD that lies somewhere within this spectrum depending on the extent of solvation. A simple experimental setup such as this allows for core-corona dimensions to be modeled since the hydrophobic core will have a different extent of solvation compared to the hydrophilic corona. Selective deuteration opens many possibilities for structural characterization and methods of determining dynamic solution behaviors, fine examples of which can be seen in the works of the Lodge group (Lu et al. 2012, 2015, 2016).

15.2.2 Pharmaceutically Relevant Structural Considerations of Self-Assembled Carriers

Besides effective delivery of drugs, there are aspects of drug behavior on the nanoscale that are important to the pharmaceutical researcher. For example, while it can be easily observed that a chemical entity once PEGylated gains water solubility (Harris et al. 2012; Veronese and Mero 2012), the conformation that clusters of the amphiphilic molecule adopt in solution has implications on how the drug will exist and act in the body.

For example, it has been shown in computational analyses that each PEG repeat unit can bind at least two water molecules which end up forming a hydrated corona around the molecule (Rissanen et al. 2014). Increased hydration due to PEG chains, however, leads to an increased entropic barrier for entering a lipid bilayer. Furthermore, this hydration increases association of Na^+ ions which compounds repulsive forces between drug

conjugates and cellular membranes as demonstrated by modeled computations of distance between PEGylated (~2000 Da PEG) biochanin and tetrahydroxyphenylporphyrin (THPP) drug conjugates and a modeled 1-palmitoyl-2-oleoylphosphatidylcholine (POPC) lipid bilayer (Rissanen et al. 2014). The results from these studies demonstrated that exposed hydrophobic portions of the PEG-THPP conjugates had solvent accessible surface areas (SASA) of 54–57% depending on the presence or absence of 140 mM NaCl while the PEG-biochanin conjugates had SASAs of only 41–45% in the same conditions. Higher SASA helped to locate the PEG-THPP conjugates on or near the modeled membrane, with typical distances of 0.8–1 nm from the membrane center, while PEG-biochanin conjugates more extensively wrapped with a PEG corona (lower SASA) associated more Na^+ ions which prevented any association with the POPC membrane.

Stopped-flow SANS was used in a related kinetic study of the interaction of amphotericin B-sodium cholesteryl sulfate (AmB-SCS) ellipsoidal micelles (45 × 2.5 nm) with 100 nm POPC-cholesterol vesicles as model 3D membranes (Foglia et al. 2015). Incorporation of SCS into the micelle decreased the time to swell the POPC-cholesterol vesicles by 0.5 nm (indication of the interaction) to 5 s vs 25 min for SCS-free micelles. It should be clear from these illustrations how information on the sizes of the core and corona in drug conjugates and the creative use of powerful SAS techniques can significantly enhance the quality of results obtained from development research.

Size characterizations such as dynamic light scattering (DLS) can give information on the size of assemblies, but with proper sample preparation, SAS studies enable "visualization" of the core and corona with nanometer accuracy and therefore give much deeper insight into the adopted conformation of the vehicle. In fact, the interior structure of an intricate self-assembled poly-ion complex system was precisely characterized using contrast variation (CV) SAXS in a study that depicted the particle morphology as a function of the ratio of cationic to neutral repeat units in a copolymer (Sakamoto et al. 2014). This investigation elegantly used form factor analysis of SAXS curves of the copolymer dispersion in water to elucidate the morphology as micelle- or vesicle-like. In addition, CV SAXS performed in a series of 5–20% PEG/H_2O solvent systems yielded electron density profiles of the vesicular structures from simultaneous model fitting of the scattering curves at different solvent contrasts. The model fitting allowed extremely precise analysis of the vesicle structure: a compact 18 nm diameter core with a 4 nm thick coronal layer and 100 nm thick hydrated shell. One of the interesting features of SAS studies such as this is the exposition of radial electron density that shows gradients of hydration. Micelles, for example, are often depicted with a strictly hydrophobic and hydrophilic region, and techniques such as DLS that reveal only size distribution cannot resolve the picture any further. However, CV SAXS and CV SANS reveal a clearer picture of the non-uniform nature of each structural component, with micelles that have interpenetrating hydrophilic polymers in the core and a shell that slowly becomes more hydrated as the polymers stretch out into the solvent.

While DLS and SAS are often complementary techniques, going from DLS to SANS characterization of the same drug-loaded micelle means going from knowing the size distribution and polydispersity of the particle to knowing such details as the intermixing of hydrophobic and hydrophilic sections when drugs are present and absent. For example, two SAXS studies on the partially benzyl esterified poly(aspartic acid)-PEG block copolymer PEG-P(Asp(Bzl)) found differing behaviors of the hydrophobic core upon loading of drug mimics of various hydrophobicities (Akiba et al. 2010; Sanada et al. 2013). Model fitting of scattering curves showed that the more hydrophobic retinoid LE540 was shown to increase the radius of the core from 5.9 to 6.9 nm when the weight % of the drug mimic in the micelle was increased from 0 to 8.3%. In analysis of a linear-linear scattering curve at high q (Fig. 15.5), the decrease of a characteristic ordering peak prompted the

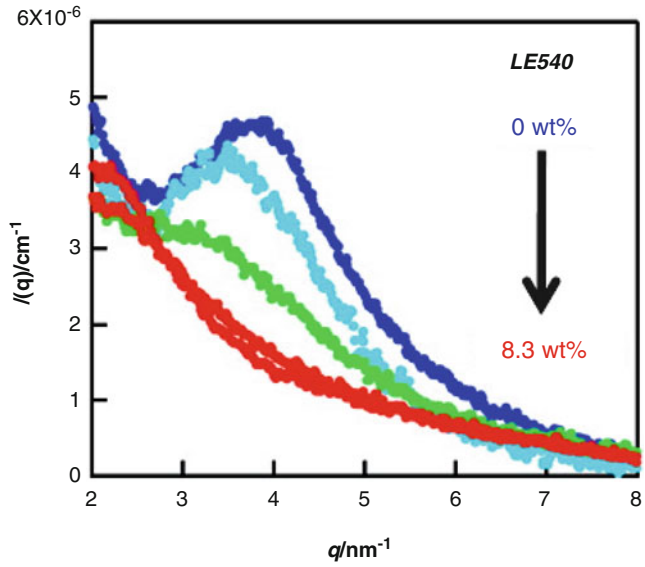

Fig. 15.5 Linear-linear plot of decreasing ordering from LE540 displacing hexagonal chain arrangement (Reprinted with permission from Akiba et al. 2010, copyright American Chemical Society)

discovery that a decrease in ordering of the core occurred as the LE540 concentration increased (Sanada et al. 2013). This result was taken to be indicative that the drug mimic was uniformly dispersed throughout the core which interrupted the interchain ordering from the aspartate groups.

In contrast, using the less hydrophobic cargo molecule tetrabromocatechol (TBC) caused no appreciable growth of the core, but anomalous SAXS showed that the TBC concentration sphere extended slightly into the hydrophilic PEG region (Akiba et al. 2010). The highly precise characterizations from both of these studies, which are uniquely available through SAS, led to the significant conclusion that the relative hydrophobicity of the cargo plays a critical role in influencing the micelle morphology, even revealing that cargo molecules may exist in both micellar regions to a small extent based on the relative hydrophobicity.

The architecture of micelles in different backbone-selective solvents is also an interesting topic that has been addressed with SANS (Alexander et al. 2014). In the investigation of grafted polyisoprene(PIP)-*g*-Pluronic polymers (where *Pluronic* is a trade name for PEO-poly(propylene oxide)-PEO triblock copolymers), the micelle architecture in solvent systems of mixed polymer selectivity (ethanol: Pluronic-selective, hexane: backbone-selective, THF: good solvent for both) was characterized to gain understanding on the solution behavior of the micelles. The contrast between deuterated solvents and hydrogenated polymers was used in model fitting to elucidate the structures. For PIP-*g*-P123 in 100% EtOH, fuzzy micelles with 16.5 nm PIP cores and 7.3 nm thick P123 chain coronas were formed. One hundred percent hexane did not produce stable particles, and after iterative solvent trials it was found that 40% THF/hexane was able to produce stable flower-like micelles with 6.4 nm P123 cores and 15.5 nm thick PIP loops in the corona. Although CV techniques are powerful as addressed above, intensive model analysis can sometimes provide similar results. In the case of the PIP-*g*-Pluronic micelles, the core and coronas were separated by their solvation densities from within model fitting analysis to provide the thicknesses.

15.2.3 Drugs

The solubility of drugs plays a key role in their behavior in and out of the body as well as in their bioavailability. For example, the loading of hydrophobic drugs into drug delivery nano-

carriers is a common way to increase their water solubility but the mechanism of drug entrapment is often assumed because it is not easily characterized without precise information on the drug's localization in the nanocarrier (Yokoyama et al. 1996).

It is clear that SAS can help illuminate the answers to these questions, but it is also used for more complex characterizations. SAS studies have been used to find the kinetics of drug release from conjugates, drug/polymer co-crystallization and association characteristics, and the relationship between conformation of formulations and their respective efficacy (Zhu et al. 2011; Paul et al. 2007; Vicent et al. 2005). For instance, time-resolved SAXS showed that the lamellar long period of 3300 Da PEG increased by 5 nm when co-crystallized with 20% benzocaine, visualized by a low q peak around 0.04 nm^{-1} that increased in size over 30 min (Zhu et al. 2011). After 24 h, this peak reduced to nothing as benzocaine was expelled from the PEG and the long period returned to 11.6 nm, close to the value of pure PEG of 11.4 nm. Ibuprofen at the same concentration was found to increase the PEG long period by 4.9 nm but as the drug crystallized separately, it was rapidly excluded from the PEG lamellae after 100 min.

In a separate study, the inclusion of a targeting ligand, galactosamine, on a polymer-drug conjugate was shown to drastically change its maximum tolerated dose (MTD). To evaluate the effect of the ligand on the in-solution conformation, solutions of 30 kDa 2-hydroxypropylmethacrylamide (HPMA)-doxorubicin (DOX) and HPMA-DOX-galactosamine in D_2O were analyzed with USANS (Vicent et al. 2005). Fitting of Gaussian coil models to the scattering data showed that the formulation containing galactosamine had a larger R_g of 9.0 nm compared to that of the standard HPMA-DOX conjugate of 7.8 nm. While both conjugates showed the same overall antitumor activity and total release of DOX, the larger R_g of the targeted conjugate was hypothesized to be responsible for the lower MTD as it indicated a more open solution geometry which allowed greater exposure of the drug to the biological locale.

15.3 SAS Studies of Drugs and Drug Delivery Vehicles

15.3.1 Nanoparticles and Micelles

One of the caveats of inorganic and drug nanoparticle preparation is the need to stabilize the particles by attaching organic molecules or polymers to their surfaces. The choice of stabilizer obviously has significant effects on the morphology and efficacy of the drug nanoparticle agent and several studies have therefore identified relevant drug-stabilizer interactions to develop rational design approaches (Choi et al. 2013; Ghosh Chaudhuri and Paria 2012).

Detailed structural analysis of the adsorption of polymers on nanoparticles is therefore an important endeavor but is only feasible through SAS. To address this, hydroxypropylcellulose (HPC)-coated nabumetone and halofantrine particles 300 nm in size were prepared and analyzed in a CV SANS experiment to gain further understanding of polymer-drug adsorption parameters (Goodwin et al. 2013). Tabulated nabumetone and halofantrine SLDs were used to initiate CV calibration and the respective D_2O/H_2O ratios of 31.3 and 33.8% were found to match the drug suspensions and agree with the tabulated values. CV SANS studies in these solvent ratios therefore eliminated scattering due to the drug core from the form factor $P(q)$ and enabled strict characterization of the adsorbed HPC corona. First, a relationship between the known R_g of free HPC of molecular weights ranging from 47 to 110 kDa and the thickness of the respective coronas was established which showed that adsorbed layers may approach thicknesses nearing the R_g (Goodwin et al. 2013). However, the adsorbed layers were found to have thicknesses below the R_g which implied that the polymers were attaching to the surface in a compacted state. For example, the R_g of 110 kDa HPC was measured to be 23.9 nm while the thickness of its nanoparticle corona layer was only 15.4 nm.

Interestingly, the molecular weight was not found to proportionally affect the layer thickness,

as polymer R_g values between 16 and 24 nm (M_W 47–110 kDa) resulted in layer thicknesses that varied randomly between 11.2 and 15.4 nm. This indicated that some of the lower molecular weight HPC adopted a less condensed conformation at the nanoparticle surface. This example shows how model fitting analysis can be effectively used to characterize the polymer-stabilized surface of micellar structures, but model-free analysis is a more concrete tool for analyzing scattering curves. Its use in conjunction with model fitting will be discussed in the next example.

In an investigation of DNA-coated gold nanoparticles (NPs), the effect of ionic strength on the architecture of 15-mer polythymine coated NPs (named T15) and 15-mer mixed sequence of 7 polythymine-CTCATGAG coated NPs (named T7–8) was characterized with SAXS/SANS (Yang et al. 2015b). This approach demonstrates intelligent solutions to some of the considerations of using both X-rays and neutrons. First, the X-ray scattering of coated metal NPs is dominated by the scattering due to the metal because of its much higher electron density in comparison to the organic molecules, which makes elucidation of coronal parameters such as thickness and chain conformation difficult (Von White et al. 2011). Therefore, SAXS was used to evaluate core parameters such as size and polydispersity independently; finding these values allowed fixing of those particular parameters during model fitting of SANS data, where, since neutron SLD values are not dependent on the size of the nucleus, core and corona scattering would not be highly differentiated between gold and DNA.

Guinier analysis of SANS curves at minimum q was used to find the R_g of the particles with T15 and T7–8 equaling 9.06 and 9.03 nm, respectively. These values were slightly higher than those found with DLS; this is a good place to note that the Guinier approximation, being made in the assumption of sufficient dilution ($S(q) \sim 1$ so $I(q)=P(q)$), is sensitive to interparticle interactions that give rise to structure factor $S(q)$ scattering. In light of this, indirect Fourier transform (IFT) analysis was used to populate a pair distance distribution function (PDDF), from which the R_g values of 8.80 and 8.79 nm for the T15 and T7–8 NPs, respectively, agreed with DLS measurements.

After the addition of 0.5 M NaCl, the PDDF of T15 retained a bell shape indicative of spherical geometry but shifted to reveal an R_g value of 8.34 nm. The T7–8 sample was found to increase in size to 13.21 nm at the same salt concentration. Interestingly, at 1 M NaCl, the R_g of T15 decreased to 8.21 nm but T7–8 aggregated which resulted in separate peaks in the PDDF. DLS data confirmed the IFT indication of aggregates.

Finally, model fitting revealed a decrease in coronal thickness for T15 from 6.58 to 5.91 nm after addition of 1 M NaCl. The most interesting analysis came from this result, where the difference between the SLD of the solvated corona and solvent was found to be 3.4×10^{-7} Å^{-2} at both 0.5 and 1 M salt concentrations. Since the shell decreased in size, the contrast difference would be expected to increase as solvent was excluded from the DNA chain. However, a constant SLD indicated that the material density of the corona increased; in other words, the solvent density was higher in the corona than in the bulk solvent. This study is an excellent example of the extremely interesting nanoscale results that can be illuminated by well-designed SAXS/SANS experiments and model-free/modeled scattering analyses.

A final example of model-free nanoparticle analysis is the SANS study of single chain nanoparticles (SCNP) in which the gap between current efforts and the goal of synthetic, globule-state, protein-like nanomachines is demonstrated (Pomposo et al. 2014). In general, the goal of SCNP research is to produce a synthetic polymer that, by carrying out the crosslinking in such a way as to eliminate interchain crosslinks in favor of purely intrachain linkages, can adopt a compact globular state. Computer simulations and SAXS/SANS data of poly(methyl methacrylate) (PMMA) SCNPs with 20 mol% reactive groups pointed to particles in an open state. The clearest presentation of the difference between SCNPs and true compact globules is presented in a Kratky plot from this study (Fig. 15.6) which shows the PMMA SCNP curve resembling

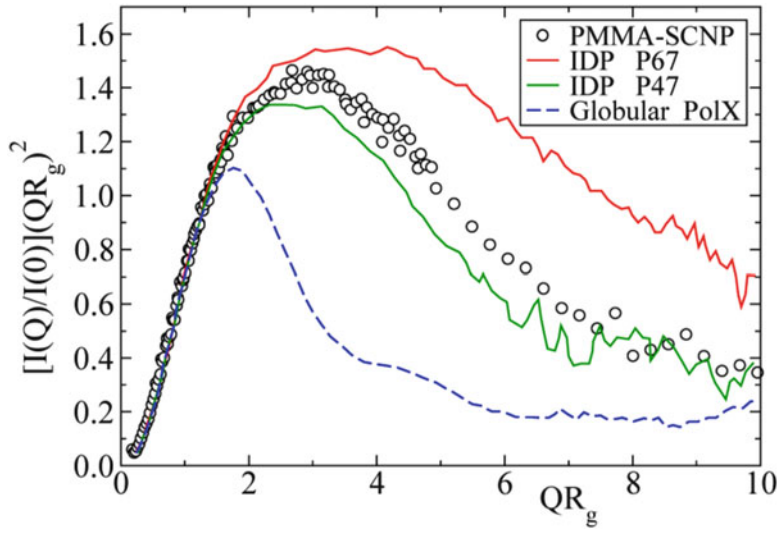

Fig. 15.6 Kratky plot of the SCNPs compared to a true globular protein and various intrinsically disordered proteins (IDPs) with open solution geometries (Reprinted with permission from Pomposo et al. 2014 copyright (2014) the American Chemical Society)

those of intrinsically disordered proteins and lacking the characteristic sharp curve of globular scattering objects. This should serve as a good example for why Kratky plots are so useful in SAS research: the Kratky plot provides quick, model-free, clear presentation of chain/particle conformation.

Although micelles are well established delivery candidates, structural studies are being carried out on even classic examples like poly(lactic acid)-poly(ethylene glycol) (PLA-PEG) micelles (Riley et al. 2003) and the poly(lactic-co-glycolide)-poly(ethylene glycol) (PLGA-PEG) system employed in one study to create micelle-like nanoparticles (Yang et al. 2015a). While the diameter of the particles was in the range of 186 nm from nanoprecipitation in THF/H_2O as observed using DLS, information on the internal particle structure was only obtainable through CV SANS which was collected using 70 and 100% D_2O in simultaneous fits (Yang et al. 2015a).

The characterization of the hydrophobic core was separated from the overall particle dimension *via* CV SANS which elucidated the core as a 7–9 nm PLGA sphere. The DLS and CV SANS R_g values were in good agreement averaging ~98 nm for particles prepared in THF/H_2O. The size results provided validation for the use of SANS to characterize these particles. A total particle R_g of ~98 nm with a core sized at only 7 nm in radius would seem to suggest a micelle with a giant corona in comparison to the core. A detailed and advanced modeling of the CV SANS data was able to reveal the large 180 nm diameter particle as a hydrophilic PEG/water environment with a fractal arrangement of multiple PLGA/PEG micelles (Fig. 15.7). It should be noted that this eventual conclusion was drawn through multiple-trial fitting routines of different models when describing the assemblies as simple spherical core-shells or solid multicomponent particles did not give reasonable conclusions.

As is often the case in SAS studies, detailed modeling is complex and iterative. For example, in one study of hexaethylene glycol monododecyl ether ($C_{12}E_6$) micelles prepared by simply mixing the surfactant in D_2O, four separate models including rounded elliptical rod, 3-axial ellipsoid, polydisperse sphere, and ellipsoid of revolution were fit to the scattering data and all showed reasonable agreement (Gapiński et al. 2010). For each model, the calculated diffusion coefficients from the dimensions were compared to DLS and fluorescence correlation spectroscopy (FCS) results before finally agreeing on the morphology of a rounded rod with elliptical

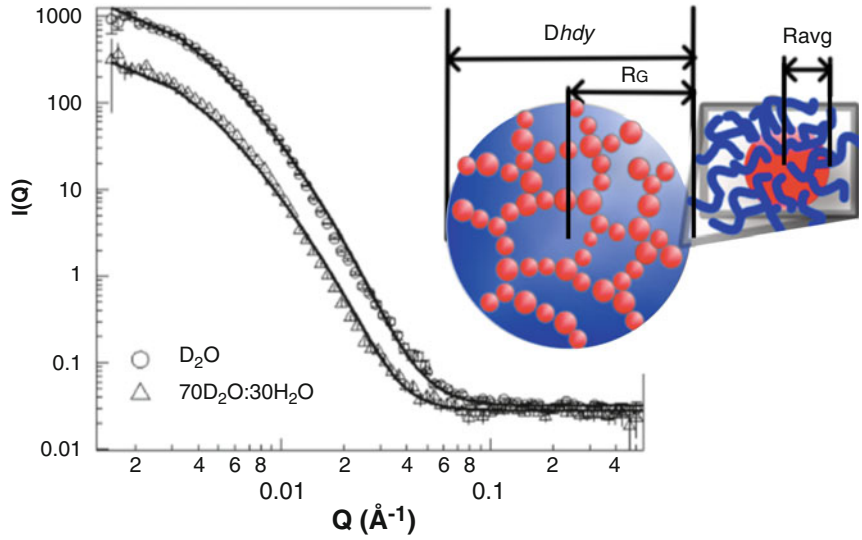

Fig. 15.7 CV SANS on PLGA-PEG nanoparticles used to elucidate the structure as fractal micelles forming a nanoparticle (Reprinted with permission from Yang et al. 2015a, copyright American Chemical Society)

cross-section resulting in the dimensions of L = 6.8 nm, a = 2.55 nm, b = 1.95 nm.

While other characterization techniques are often used to support SAS studies, as demonstrated above, SAS is equally used to validate the results from physical characterizations such as transmission electron microscopy (TEM). For example, pixel analysis of cryo-TEM images was used to determine the coronal dimension of micelles formed from pincer-ligand end-functionalized poly(N-isopropylacrylamide) (PNIPAM) of 20 kDa in water (Patterson et al. 2013). However, to validate this method and extend the characterization, SANS curves from mixing the polymer in D_2O were fit with core-shell models including a corona of radially decreasing hydration. The cryo-TEM image analysis identified the micelles as ~20 nm spheres, which agreed with DLS results. The SANS results extended this characterization to a 1–2 nm core with 18–20 nm corona. Interestingly, the core size from SANS was indicative of a fully extended C_{12} chain, which was consistent with the size of the end-functional pincer ligand. It should be noted that SANS is an ensemble technique; scattering from a sample represents an average of all the constituents of that sample. It therefore gives a representative picture of the size and shape of all the particles in solution, in contrast to techniques like cryo-TEM which offer direct imaging of a very localized scope. Using both techniques in parallel offers the best range of size scales and the most complete level of precision.

In a characterization of simpler PLA/PEG micelles, the PLA core could be modeled as homogenous with a constant SLD (Riley et al. 2003). However, the PEG shell was better modeled by an SLD that decreased radially from the core as the polymer became hydrated to the point of equaling the solvent in SLD. This accurate model based on contrast variation was used to show that the micelle radius increased from 16 to 54.5 nm as the ratio of PLA:PEG repeat units increased from 3:5 to 45:5 and that the thickness, structure, and density of the PEG layer depended on the same parameter. CV SANS was used to isolate the core parameters from the overall scattering by subtracting the shell from the overall size. In the case of the PLA/PEG micelles, different solvent ratios and pure polymers were scanned as building blocks for the CV analysis (Fig. 15.8).

It should be noted, however, especially considering these successful characterizations through CV SANS, that the actual experimental

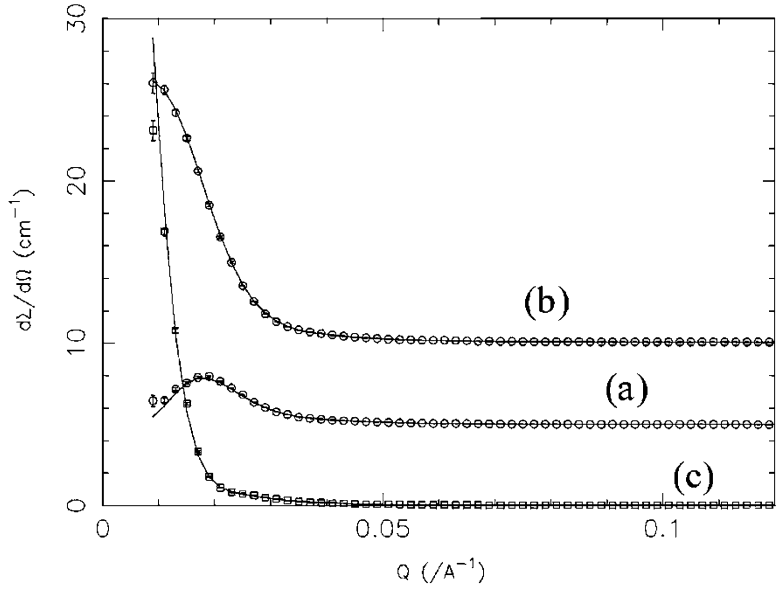

Fig. 15.8 CV SANS on mixed solvents showing the range of SLDs obtainable and the scattering due to PLA(D)-PEG 15:5 micelles at (*a*) 100% D_2O, (*b*) 80% D_2O, (*c*) 65% D_2O (Reprinted with permission from Riley et al. 2003, copyright American Chemical Society)

case of contrast management is slightly more complicated than the usual diagram depictions and results sections may appear. What would be expected to be acutely disparate contrast differences (i.e. hydrophobic core/hydrophilic shell) are in reality blurred by factors like chain exchange, core interpenetration, and partial hydration (Patterson et al. 2013; Lu et al. 2016). Thus, in an effort to clarify the properties affecting chain exchange, polystyrene (PS)- poly(ethylene-*alt*-propylene) (PEP) block copolymers were assembled into micelles in the PEP-selective solvent squalane in thoughtfully designed CV SANS studies which monitored dynamic contrast over time to evaluate the kinetics of chain exchange (Lu et al. 2015, 2016). The experimental design in these studies is a wonderful example of inventive CV SANS use. Firstly, PS-PEP-PS and PEP-PS-PEP triblock copolymers with comparable solvophilic PEP blocks form micelles in squalane, with the former resulting in flower-like micelles with PEP loops extending from the core and the latter forming the classic fuzzy micelles with PEP chains extending from the core. The molecular weight of the copolymers was ~230 kDa, with PEP blocks of ~140 kDa. Standard copolymers and identical versions with perdeuterated PS blocks were prepared as micelles in the solvent and dried before being mixed in equal ratios. The inventive concept was as follows: when the dried, pure-core micelles, half containing hydrogenated PS and half containing deuterated PS, were suspended in a 58% D-squalane/H-squalane solvent mixture which has an SLD matching that of a perfectly mixed PS core, the initial contrast from the pure micelle cores, which is given by the contrast factor $I \sim (SLD_{d,core}\text{-}SLD_{h,core})^2$ would be at a maximum value and would decay to zero as the chains exchanged and eventually cause evenly mixed cores (Lu et al. 2012). From time resolved (TR) SANS studies on these micelles it was found that the exchange rate of PS-PEP-PS micelles was nine orders of magnitude greater than the PEP-PS-PEP micelles which resulted in the conclusion that the rate limiting

mechanism was the extraction of PS block cores into the solvent.

15.3.2 Vesicles

The ability of delivery vehicles to entrap and release drugs of various hydrophobicities is correlated to the carrier structure (Chemelli et al. 2012; Nguyen et al. 2011). In this regard, stimuli responsive shape change in a drug carrier offers a viable mechanism for controlled delivery. However, detailed characterization of these shape changes is crucial for understanding and optimizing the mechanism of delivery.

Using pH change as a stimulus, nicergoline/glycerol monooleate (GMO) colloids prepared by sonication of both solids (5 w/w% total, nicergoline varied between 10 and 30 wt%) in 1% Pluronic F108/water were found to have pH-dependent morphology, switching from vesicles to inverse micelles during a change from below pH = 5.1 to above pH = 6.6 (Salentinig et al. 2014). GMO bearing a relatively small C_{17} chain resulted in micelles 4 nm in diameter when the nicergoline concentration was >20% at pH >6.6, with the nicergoline entrapped in the center.

However, nicergoline has multiple lone-pair nitrogens that can be protonated at different pH values and is responsible for the pH-driven shape change. Using crystallographic parameters outside the scope of this description allowed the determination of the apparent pK_a of the nicergoline-GMO system. Generalized IFT from q >0.09 $Å^{-1}$ was used to provide a PDDF that characterized the size and shape of the nano-objects and revealed that the monooleate bilayer of the vesicle resulting from shifting the pH <5.1 was 5 nm in thickness.

This type of analysis for vesicle bilayers, or generically, locally flat sheets with respect to the scattering range of q, from thickness PDDF plots is an analysis shown in early SAXS works by Glatter (Glatter 1980; Glatter and Hainisch 1984). In these crystallographic studies, Glatter worked with simulated scattering data to develop mathematical analysis techniques for interpreting physical parameters of solid objects. It was shown that deconvolution using a function he derived allows radial electron density profiles to be calculated. Electron densities within the particle radius can thusly reveal the thickness of interlayers and their molecular ordering (crystallographic unit cell packing parameters) in addition to providing information on the location of drug molecules as shown in this study. For example, the packing of GMO was found from Bragg reflections in the scattering data to be indicative of Pn3m cubosomes and hexosomes, which shifted to an *Im3m* bicontinuous cubic phase as pH went from >8.0 to <7.0.

Further, radially dependent electron density moving outward from the micellar monooleate core was also used to evaluate the water hydration sphere in the glycerol corona. From the examples in this study, along with the chain exchange, solvent selective morphology, and drug effect on micelle conformation studies discussed in the previous section it can be seen that questions concerning self-assembly are being addressed very quantitatively with SAS techniques.

Vesicles, owing to their unique architecture and larger size compared to micelles, are often the focus of studies aiming to uncover details about the hydrophobic layer or bilayer. The first important consideration for vesicles is that their size can easily exceed 1 μm and, therefore, the range of q in scattering studies is not low enough to encompass the Guinier region (Borchert et al. 2006). Instead, the scattering intensity in the reasonable q range of the instrument is best approximated by that due to a flat sheet. For vesicles this enables detailed analysis of the hydrophobic interlayer when CV conditions or modeling analyses are used.

For example, the bilayer thickness of poly (2-vinylpyridine-*b*-ethylene oxide) (PVP-PEO) block copolymer vesicles 1–10 μm in diameter formed from nanoprecipitation in $CHCl_3/H_2O$ was evaluated with SANS in D_2O (Rubner and Cohen n.d.). The PVP polymer contains ionizable nitrogens that render the polymer insoluble above the pK_a and result in the formation of vesicles. By fitting scattering data in the q range

of 0.005–0.05 $Å^{-1}$, the PVP bilayer thickness of vesicles formed from PVP-PEO copolymers with ~30, 40, and 70 PVP units at pH >5 was found to be 10.7, 13.6, and 13.5 nm, respectively.

Similarly, in an investigation of polydimethylsiloxane-*g*-poly(ethylene oxide) (PDMS-*g*-PEO) graft polymers and PEO-PDMS-PEO triblock copolymers, the hydrophobic bilayer was characterized using SANS in D_2O (Salva et al. 2013). The vesicles were prepared by mixing the polymers in water and extruding 19 times through 0.1 μm filters. However, cryo-TEM still revealed large, polydisperse vesicles which caused oscillations at low q such that quantification in that range was not possible. However, modeling of the scattering curves revealed an average of 33 nm PEO cores with 5.75 nm PDMS bilayer membranes and 15 nm outer shells. An interesting use of a log-log scaled Kratky plot was also utilized for intermediate q in which $\pi/qmax$ (the local maximum of intermediate q) provided the characteristic length of the membrane, 6.0 nm, which agreed well with the model fitting analysis.

For the PEO-PDMS-PEO triblock copolymers, high polydispersity disrupted higher q such that the log scaled Kratky plot was not useful. However, the slope of the fit line from a Kratky-Porod plot of $\ln(Iq^2)$ vs q^2 provided the membrane thickness as 11 nm which agreed with cryo-TEM images. Model fitting of the entire curve gave a core of 14.9 nm with a PDMS interlayer membrane of 11.4 nm and a 26.5 nm hydrated PEO outer corona, giving a final agreement for multiple analyses.

While the two studies discussed above focused on the characteristics of the vesicle membrane as a homogenous entity, there are a number of works focused on investigating small nano-domains within vesicle walls. The nanodomains have completely different form factors compared to the assumed flat sheet of the vesicle surfaces which make them difficult to analyze without SAS. Similar principles to those in the studies above apply: that in a polydisperse system of large spheres, surface curvature can be neglected and the scattering is treated as coming from randomly dispersed flat surfaces (Vogtt et al. 2010).

In a study of vesicles formed from multiple extrusions of a mixed lipid system (molar ratio of 45:27:28 DOPC:DPPC-d62:cholesterol) through 30-nm filters in water, CV SANS in D_2O/H_2O was used to characterize the vesicles as 14.5 nm spheres with 2.5 nm bilayers. Selection of a single deuterated component and a contrast matched D_2O/H_2O solvent system also allowed characterization of small nanodomains in the disordered liquid phase as flat cylinders 2.5 nm long with a radius of 14.5 nm. This general flattened shape was confirmed from the low q behavior of the log-log scattering curve in the region of $0.1 < q < 1.5\ nm^{-1}$ where the scattering curve displayed q^{-2} dependence indicative of flat objects.

The formation of nanodomains is not limited to vesicles composed purely of lipids, as demonstrated by the study of grafted PDMS-g-PEG mixed with DPPC/POPC (50:50) ratio to form 80:20 polymer:lipid vesicles (Dao et al. 2015). In this work, thin film rehydration/extrusion through 100-nm pores was used to create vesicles 52 nm in diameter. CV SANS in 10% D_2O/H_2O provided PDMS-matched conditions in which independent observation of the lipids was possible, while 80% D_2O/H_2O matched the SLD of the lipids and allowed polymer "visualization" in the SANS curve. From Kratky-Porod plots the vesicle membrane thickness was found to be 5.8 nm, but the vesicle model was found to be insufficient for the lipid-matched polymer scattering curves. Instead, the polydisperse flat cylinder model was found to describe the polymer nanodomains as 30 nm radius, 5.1 nm length cylinders. It should be noted that the apparent size of the flat cylinders from the model does not seem reasonable considering the diameter of the overall vesicles (~52 nm). A major consideration in this case was the polydispersity and variable content of the nanodomains and the ever-present fact that SAS curves can be acceptably fit with multiple models.

Without information from other characterization techniques it can be difficult to pinpoint some structural features in SAS modeling due

to the number of uninformed floating parameters. While characterization of the vesicle's overall structure was confirmable with DLS and shown to be reliable from several modeled approaches, characterization of the nanodomains suffered from being necessarily independent from other techniques. Both the immense strength and characteristic weaknesses of SAS can be seen in these studies.

15.3.3 Capsules

Hollow polymer capsules present one of the most interesting subjects of SAS drug delivery subjects. Firstly, they have an extremely wide range of compositional aspects that can be varied quite easily, including polymer composition, molecular weight, interlayer interaction, and size (Li et al. 2011; Shutava and Lvov 2006; Shutova et al. 2007; Zavgorodnya et al. 2015). Small nm-range sizes of capsules can be studied encompassingly with SANS which provides very interesting details on their morphology before and after template dissolution (Estrela-Lopis et al. 2002). Since polymer capsules can also exist as large particles >1 μm, very low q ranges can be needed to fully characterize their size and shape in SAS. However, when this information is gathered in other more facile ways these parameters can be included in fitting models. Following this, the ratio of shell thickness to overall particle diameter is very small, which makes characterizing the thickness accurately impossible without SAS techniques. Additionally, specific modeling and analyses such as those stemming from Kratky-Porod plots are able to shed light on this topic (Balgavy et al. 2001; Richter et al. 2011). In this regard the smallest of small angles can be fully utilized and scattering instruments can be pushed to their physical limits. For perspective, the D11 SANS instrument at Institut Laue-Langevin uses a 39 m sample-to-detector distance to separate low q range scattering measurements from the main beam.

Capsules also have the potential to be extremely monodisperse due to their templated assembly which provides highly uniform scattering in contrast to self-assembled structures that can be quite polydisperse. Common goals for SAS research on hollow capsules are finding the capsule wall thickness in solution and characterizing the interior environment (Estrela-Lopis et al. 2007). The hollow morphology of these particles means that the solvent-filled core can be modeled as equal to the bulk solvent in SLD and scattering due to the polymeric shell can be analyzed separately.

It is important to remember that scattering data may look somewhat similar and that the important conclusions come from careful modeling. For acquisitions leading to information on capsule shell thickness, fewer parameters left floating during data fitting such as particle radius, SLD of the core/shell, interparticle factors, and polydispersity lead to more accurate results when the models are being pushed. This is born from the fact that the q range of most instruments falls short of fully wrapping the scale of such objects. Polydispersity and size can be measured with DLS (Rube et al. 2005), or confocal laser scanning microscopy (Kozlovskaya et al. 2014) while the SLD value of polymeric material can be closely approximated to known values. Since polydispersity smoothens scattering profiles quite effectively, having guidelines for these parameters can enhance model accuracy for other parameters such as core size which can be independently measured by scanning electron microscopy (Chen et al. 2013) and shell thickness which can be determined by atomic force microscopy (AFM) (Liu et al. 2014; Espinosa-Dzib et al. 2015). Outside of some of the more advanced modeling routines, a good example of model-free analysis is the modified Guinier plot which can give bilayer thickness of vesicles (Kim et al. 2014) from the slope of $\ln(Iq^2)$ vs q^2 in the Guinier thickness range (Fig. 15.9).

Analyses such as these have also been conducted on polyelectrolyte multilayer capsules made *via* ionic pairing of poly(styrene sulfonate) with poly(allylamine hydrochloride) (PSS/PAH) and ranging from 130 nm to 3 μm in size for separate samples with successful modeling of

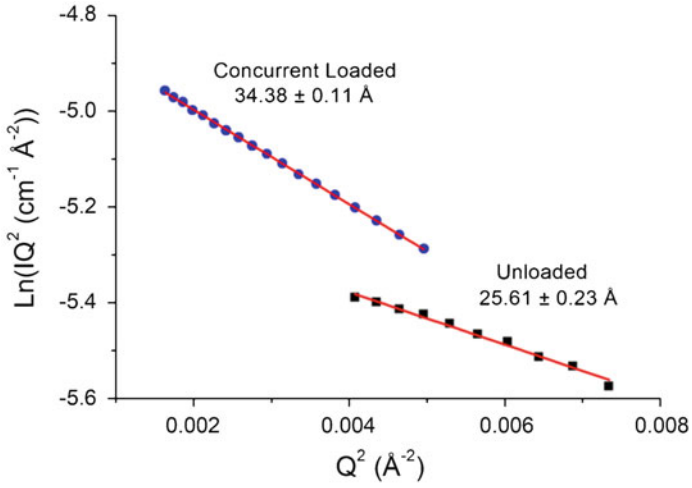

Fig. 15.9 Modified Guinier plot with linear fits giving R_g which can be used to calculate shell thickness (Reprinted with permission from Kim et al. 2014, copyright American Chemical Society)

capsule wall thicknesses (Estrela-Lopis et al. 2009). The capsules in this study were modeled as core-shell particles, and removal of interparticle structure factors (by sufficient dilution) allowed isolation of the form factors representing scattering from the core, core-shell interface, and shell polymers.

As mentioned, for hollow capsules a core-shell model where the core matches the solvent in SLD can be used to isolate scattering from the polymer shell. However, analysis of scattering from separate samples with reserved core templates enabled the conclusion that supported shell layers, i.e., those still standing on the templates, are 25% thinner than free capsule shells, i.e., those with templates having been dissolved (Balgavý et al. 2001). While this result may seem intuitive, it is quite significant in that SANS is one of the only ways to characterize detailed shell swelling and prove this reasonable hypothesis.

Moreover, the hydration of the $(PSS/PAH)_{8,12,16}$ shells where the subscript denotes the number of PSS/PAH polymer bilayers within the capsule shell was determined to be higher in freestanding layers (52%) compared to template-bound layers (42%) from the difference in SLD of hydrated polymers compared to pure solvent (Balgavý et al. 2001). The thickness of PSS/PAH capsule shells in solution, found from SANS analysis to be ~2 nm per PSS/PAH bilayer, was found to be in agreement with the thickness of collapsed capsules in the dry state found using AFM.

However, AFM thickness data cannot always accurately approximate thicknesses of hydrated layers. For example, in a study of PSS/PAH multilayer capsules formed on red blood cells, AFM measurements revealed capsule wall thickness that were artificially higher than the thickness measured with SANS (Estrela-Lopis et al. 2007). In this work, six bilayers of PSS/PAH were found from modeled SANS data to have a total thickness of only 4.5 nm, while AFM results were much higher. The difference stems from the removal of up to 90% of the PSS during core removal, which was shown to be trapped within the core with SANS. However, when drying the capsule suspension for AFM it was hypothesized that the PSS trapped in the core contributed to the height found from the AFM probe. These results are a significant example of how SANS can validate results brought to hypothesis from other techniques, while also shedding light on the intrinsic weakness of other techniques that can lead to inaccurate conclusions.

Investigating the core environment of capsules is another useful application for SAS techniques where in-solution techniques like DLS are not sensitive to scattering from the

object's interior (Lof et al. 2007). For encapsulated biological macromolecules that contain metals, SAXS is particularly helpful due to the disparate contrast from the electron density of metals compared to organic molecules as shown in the characterization of hemoglobin inside $(\text{chitosan/alginate})_{10}$ capsules (Mandal et al. 2012). In this study, the aggregation of hemoglobin inside the capsules compared to free hemoglobin in solution was compared to evaluate the effect of encapsulation on redox response found from cyclic voltammetry of the hemoglobin. Porod analysis was used heavily with a focus being the Porod exponent aggregation behavior.

First, a theoretical R_g for hemoglobin was established by a simulation and found to be 22.37 Å. This value was compared to the value determined from SAXS of the polymer-encapsulated hemoglobin (26.6 Å) and found to be in agreement. The more interesting result came from the experimentally determined polydispersity figure for encapsulated hemoglobin of 0.11, which was much lower than the free hemoglobin value of 0.71. This implied that the hemoglobin was highly monodisperse when encapsulated which is indicative of non-aggregation. This study is a good example of how SAXS can be used to take advantage of the increased scattering from biological macromolecules that contain or incorporate metals to evaluate their properties independently of the system in which they are being studied.

15.3.4 Drug Modeling, Behaviors, Interactions

The constant development of new drugs that are very often hydrophobic comes with the parallel development of methods to increase the solubility of these drugs. Characterizing the solubility of drugs is an effort being pursued by medicinal laboratories but often the acquisition timescale is slower than the drug dissolution species change. Powder X-ray diffraction is often used to characterize solids but available instruments typically have measurement timescales around 10 min. Efforts to elucidate more detail in shorter time intervals for rapidly solubilizing or crystallizing drugs are being supported by the speed and resolution of SAXS (Boetker et al. 2012), with intermediate species and kinetics being discovered from this technique. Both anhydrous and monohydrate forms of theophylline were characterized kinetically during dissolution and recrystallization using SAXS at complete experimental timescales under 100 s.

At the other end of the spectrum, encapsulating protein drugs is an application that has potential for drug delivery (Besanger et al. 2004; Ciriminna et al. 2013; Zeno et al. 2014). However, characterizing the encapsulated proteins is not simple using optical techniques. Instead, CV SANS and deuterated proteins were used in a study of green fluorescent protein *in silica* sol-gels to evaluate the conformation of the protein and its effects on the structure of the gel (Luo et al. 2009). The mixed solvent system of 60% D_2O/H_2O was found to match silica which allowed direct access to scattering from the protein, while 42% D_2O was used to match hydrogenated protein and evaluate scattering from the silica matrix. From simultaneous fits of SANS data at 0, 30, and 100% D_2O the typical particle size in the silica sol-gel was found to have a radius of 13.73 Å with pores having a radius of 33.69 Å. Entrapment of the protein did not significantly change the particle size (12.24 Å) but was shown to increase the pore size significantly to 66.01 Å. A Fourier transform approach from the silica-matched SANS curve with deuterated protein to increase the contrast without having to significantly increase protein concentration allowed the elucidation of protein quaternary structure to be an end-to-end dimer.

15.4 Conclusions and Practical Tips

SAS techniques are powerful tools to the researchers looking to discover the most fundamental details of drug delivery systems. The elucidation of these details has rapidly increased

the knowledge available to polymer, material, and pharmaceutical researchers over the last decade. While other techniques have allowed discovery of information about the size and dispersity of nanometer sized particles, SAS has helped answer questions that will likely increase the efficiency of drug delivery systems moving forward. However, as the subjects of SAS studies continue to increase in complexity, the instrumental techniques are also increasing in power, resolution, etc. The proliferation of USANS and USAXS instruments is heralding the characterization of larger particles while increased flux in both types of scattering sources is increasing throughput of samples and the speed of information being gained on both novel and fundamental systems.

Practical tips:

- When using model-free data analysis of the Guinier region, keep in mind that particle aggregation has a significant effect on the line slope and apparent R_g: this may provide estimates that are different than would be expected. Aggregation of particles also effects parameters in model fitting in ways that are not always apparent. For instance, aggregation increases polydispersity which intuitively affects the apparent particle size, but can decrease the apparent shell thickness for core-shell models.
- SAS characterizations of drug delivery particles and systems provide the most reliable data only when supplemented with as many other techniques as possible. Model parameters that can be fixed due to prior knowledge make the model fit more accurate. Model-free analyses give the best results when they are informed by relevant physical characterizations. The same scattering data can be fit equally well by many completely unrelated models.
- Always keep the size frame of reference for SAS scattering in mind when looking at data: Porod slopes describe surfaces or fractals; Guinier region slopes describe particle shape if the particle size is measurable at that q; remember also that non-dilute samples show interparticle peaks and/or structure factor scattering.
- Conclusions drawn from SAS techniques are often the result of an iterative approach with a sizable amount of trial and error where good intuition can help clarify the results; particle scattering could be fit equally well by a fractal micelle model or one that indicates a micelle with unreasonable dimensions, such as a 2 nm core and 100 nm corona. It is left to the user to distinguish whether the conclusion is reasonable or not and to interpret the model from an informed standpoint to give reasonable results.
- Polymers, drug molecules, and polymeric materials do not always have the same behavior in D_2O and H_2O. It is best to check simple things like the solubility, R_g, and dispersity before beginning scattering experiments.

Acknowledgement This work was supported by NSF Career Award 1350370.

References

Akiba I, Terada N, Hashida S, Sakurai K, Sato T, Shiraishi K, Yokoyama M, Masunaga H, Ogawa H, Ito K, Yagi N (2010) Encapsulation of a hydrophobic drug into a polymer-micelle core explored with synchrotron SAXS. Langmuir 26(10):7544–7551

Alexander S, Cosgrove T, de Vos WM, Castle TC, Prescott SW (2014) Aggregation behavior of polyisoprene–pluronic graft copolymers in selective solvents. Langmuir 30(20):5747–5754

Almgren M, Garamus VM, Asakawa T, Jiang N (2007) Contrast variation SANS investigation of composition distributions in mixed surfactant micelles. J Phys Chem B 111(25):7133–7141

Bae JW, Lee E, Park KM, Park KD (2009) Vinyl sulfone-terminated PEG−PLLA diblock copolymer for thiol-reactive polymeric micelle. Macromolecules 42 (10):3437–3442

Balgavý P, Dubničková M, Kučerka N, Kiselev MA, Yaradaikin SP, Uhríková D (2001) Bilayer thickness and lipid interface area in unilamellar extruded 1,2-diacylphosphatidylcholine liposomes: a small-angle neutron scattering study. Biochim Biophys Acta Biomembr 1512(1):40–52

Becker AL, Johnston APR, Caruso F (2010) Layer-by-layer-assembled capsules and films for therapeutic delivery. Small 6(17):1836–1852

Besanger TR, Easwaramoorthy B, Brennan JD (2004) Entrapment of highly active membrane-bound receptors in macroporous sol−gel derived silica. Anal Chem 76(21):6470–6475

Biggs S, Labarre M, Hodges C, Walker LM, Webber GB (2007) Polymerized rodlike micelle adsorption at the solid−liquid interface. Langmuir 23 (15):8094–8102

Boetker J, Rades T, Rantanen J, Hawley A, Boyd BJ (2012) Structural elucidation of rapid solution-mediated phase transitions in pharmaceutical solids using in situ synchrotron SAXS/WAXS. Mol Pharm 9(9):2787–2791

Borchert U, Lipprandt U, Bilang M, Kimpfler A, Rank A, Peschka-Süss R, Schubert R, Lindner P, Förster S (2006) pH-induced release from P2VP−PEO block copolymer vesicles. Langmuir 22(13):5843–5847

Caruso F, Caruso RA, Möhwald H (1998) Nanoengineering of inorganic and hybrid hollow spheres by colloidal templating. Science 282 (5391):1111

Chemelli A, Maurer M, Geier R, Glatter O (2012) Optimized loading and sustained release of hydrophilic proteins from internally nanostructured particles. Langmuir 28(49):16788–16797

Chen J, Kozlovskaya V, Goins A, Campos-Gomez J, Saeed M, Kharlampieva E (2013) Biocompatible shaped particles from dried multilayer polymer capsules. Biomacromolecules 14(11):3830–3841

Cho J, Hong J, Char K, Caruso F (2006) Nanoporous block copolymer micelle/micelle multilayer films with dual optical properties. J Am Chem Soc 128 (30):9935–9942

Choi I, Malak ST, Xu W, Heller WT, Tsitsilianis C, Tsukruk VV (2013) Multicompartmental microcapsules from star copolymer micelles. Macromolecules 46(4):1425–1436

Ciriminna R, Fidalgo A, Pandarus V, Béland F, Ilharco LM, Pagliaro M (2013) The sol–gel route to advanced silica-based materials and recent applications. Chem Rev 113(8):6592–6620

Correa NM, Silber JJ, Riter RE, Levinger NE (2012) Nonaqueous polar solvents in reverse micelle systems. Chem Rev 112(8):4569–4602

Dao TPT, Fernandes F, Er-Rafik M, Salva R, Schmutz M, Brûlet A, Prieto M, Sandre O, Le Meins JF (2015) Phase separation and nanodomain formation in hybrid polymer/lipid vesicles. ACS Macro Lett 4(2):182–186

Decher G (2002) Polyelectrolyte multilayers, an overview. In: Multilayer thin films. Wiley-VCH Verlag GmbH & Co. KGaA, Weinheim, pp 1–46

Donath E, Sukhorukov GB, Caruso F, Davis SA, Möhwald H (1998) Novel hollow polymer shells by colloid-templated assembly of polyelectrolytes. Angew Chem Int Ed 37(16):2201–2205

Elsner N, Kozlovskaya V, Sukhishvili SA, Fery A (2006) pH-triggered softening of crosslinked hydrogen-bonded capsules. Soft Matter 2(11):966–972

Erel-Unal I, Sukhishvili SA (2008) Hydrogen-bonded multilayers of a neutral polymer and a polyphenol. Macromolecules 41(11):3962–3970

Espinosa-Dzib A, Chen J, Zavgorodnya O, Kozlovskaya V, Liang X, Kharlampieva E (2015) Tuning assembly and enzymatic degradation of silk/poly (N-vinylcaprolactam) multilayers *via* molecular weight and hydrophobicity. Soft Matter 11(25):5133–5145

Estrela-Lopis I, Leporatti S, Moya S, Brandt A, Donath E, Möhwald H (2002) SANS studies of polyelectrolyte multilayers on colloidal templates. Langmuir 18 (21):7861–7866

Estrela-Lopis I, Leporatti S, Typlt E, Clemens D, Donath E (2007) Small angle neutron scattering investigations (SANS) of polyelectrolyte multilayer capsules templated on human red blood cells. Langmuir 23 (13):7209–7215

Estrela-Lopis I, Leporatti S, Clemens D, Donath E (2009) Polyelectrolyte multilayer hollow capsules studied by small-angle neutron scattering (SANS). Soft Matter 5 (1):214–219

Filippov SK, Chytil P, Konarev PV, Dyakonova M, Papadakis C, Zhigunov A, Plestil J, Stepanek P, Etrych T, Ulbrich K, Svergun DI (2012) Macromolecular HPMA-based nanoparticles with cholesterol for solid-tumor targeting: detailed study of the inner structure of a highly efficient drug delivery system. Biomacromolecules 13(8):2594–2604

Filippov SK, Franklin JM, Konarev PV, Chytil P, Etrych T, Bogomolova A, Dyakonova M, Papadakis CM, Radulescu A, Ulbrich K, Stepanek P, Svergun DI (2013) Hydrolytically degradable polymer micelles for drug delivery: a SAXS/SANS kinetic study. Biomacromolecules 14(11):4061–4070

Foglia F, Rogers SE, Webster JRP, Akeroyd FA, Gascoyne KF, Lawrence MJ, Barlow DJ (2015) Neutron scattering studies of the effects of formulating amphotericin B with cholesteryl sulfate on the drug's interactions with phospholipid and phospholipid–sterol membranes. Langmuir 31(29):8042–8051

Fong WK, Hanley TL, Thierry B, Kirby N, Boyd BJ (2010) Plasmonic nanorods provide reversible control over nanostructure of self-assembled drug delivery materials. Langmuir 26(9):6136–6139

Gapiński J, Szymański J, Wilk A, Kohlbrecher J, Patkowski A, Hołyst R (2010) Size and shape of micelles studied by means of SANS, PCS, and FCS. Langmuir 26(12):9304–9314

Ghosh Chaudhuri R, Paria S (2012) Core/shell nanoparticles: classes, properties, synthesis mechanisms, characterization, and applications. Chem Rev 112(4):2373–2433

Glatter O (1980) Evaluation of small-angle scattering data from lamellar and cylindrical particles by the indirect transformation method. J Appl Crystallogr 13:577–584

Glatter O, Hainisch B (1984) Improvements in real-space deconvolution of small-angle scattering data. J Appl Crystallogr 17:435–441

Glatter O, Kratky O (1982) Small angle X-ray scattering. Academic, New York

Goodwin DJ, Sepassi S, King SM, Holland SJ, Martini LG, Lawrence MJ (2013) Characterization of polymer adsorption onto drug nanoparticles using depletion measurements and small-angle neutron scattering. Mol Pharm 10(11):4146–4158

Guinier A, Fournet G (1955) Small-angle scattering of X-rays. Wiley, New York

Hammond PT (2011) Engineering materials layer-by-layer: challenges and opportunities in multilayer assembly. AICHE J 57(11):2928–2940

Hammouda B (2010a) A new guinier porod model. J Appl Crystallogr 43:716–719

Hammouda B (2010b) Analysis of the beaucage model. J Appl Crystallogr 43:1474–1478

Hammouda B (2016) Probing nanoscale structures using neutron scattering. NIST NCNR distance learning course

Harris JM, Martin NE, Modi M (2012) Pegylation. Clin Pharmacokinet 40(7):539–551

Kharlampieva E, Sukhishvili SA (2006) Hydrogen-bonded layer-by-layer polymer films. J Macromol Sci Part C 46(4):377–395

Kharlampieva E, Kozlovskaya V, Sukhishvili SA (2009) Layer-by-layer hydrogen-bonded polymer films: from fundamentals to applications. Adv Mater 21 (30):3053–3065

Kim MD, Dergunov SA, Richter AG, Durbin J, Shmakov SN, Jia Y, Kenbeilova S, Orazbekuly Y, Kengpeiil A, Lindner E, Pingali SV, Urban VS, Weigand S, Pinkhassik E (2014) Facile directed assembly of hollow polymer nanocapsules within spontaneously formed catanionic surfactant vesicles. Langmuir 30 (24):7061–7069

Kozlovskaya V, Kharlampieva E, Erel I, Sukhishvili SA (2009) Multilayer-derived, ultrathin, stimuli-responsive hydrogels. Soft Matter 5(21):4077–4087

Kozlovskaya V, Baggett J, Godin B, Liu X, Kharlampieva E (2012a) Hydrogen-bonded multilayers of silk fibroin: from coatings to cell-mimicking shaped microcontainers. ACS Macro Lett 2012(1):384–387

Kozlovskaya V, Zavgorodnya O, Chen Y, Ellis K, Tse HM, Cui W, Thompson JA, Kharlampieva E (2012b) Ultrathin polymeric coatings based on hydrogen-bonded polyphenol for protection of pancreatic islet cells. Adv Funct Mater 22(16):3389–3398

Kozlovskaya V, Alexander JF, Wang Y, Kuncewicz T, Liu X, Godin B, Kharlampieva E (2014) Internalization of red blood cell-mimicking hydrogel capsules with pH-triggered shape responses. ACS Nano 8 (6):5725–5737

Lagzi I, Wang D, Kowalczyk B, Grzybowski BA (2010) Vesicle-to-micelle oscillations and spatial patterns. Langmuir 26(17):13770–13772

Li H, Pang S, Wu S, Feng X, Mullen K, Bubeck C (2011) Layer-by-layer assembly and UV photoreduction of graphene-polyoxometalate composite films for electronics. J Am Chem Soc 133(24):9423–9429

Lisunova MO, Drachuk I, Shchepelina OA, Anderson KD, Tsukruk VV (2011) Direct probing of micromechanical properties of hydrogen-bonded layer-by-layer microcapsule shells with different chemical compositions. Langmuir 27 (17):11157–11165

Liu F, Kozlovskaya V, Zavgorodnya O, Martinez-Lopez-C, Catledge S, Kharlampieva E (2014) Encapsulation of anticancer drug by hydrogen-bonded multilayers of tannic acid. Soft Matter 10(46):9237–9247

Liu F, Kozlovskaya V, Medipelli S, Xue B, Ahmad F, Saeed M, Cropek D, Kharlampieva E (2015) Temperature-sensitive polymersomes for controlled delivery of anticancer drugs. Chem Mater 27 (23):7945–7956

Löf D, Schillén K, Loh W, Olofsson G (2007) A calorimetry and light scattering study of the formation and shape transition of mixed micelles of EO20PO68EO20 triblock copolymer (P123) and nonionic surfactant (C12EO6). J Phys Chem B 111 (21):5911–5920

Lu J, Choi S, Bates FS, Lodge TP (2012) Molecular exchange in diblock copolymer micelles: bimodal distribution in core-block molecular weights. ACS Macro Lett 1(8):982–985

Lu J, Bates FS, Lodge TP (2015) Remarkable effect of molecular architecture on chain exchange in triblock copolymer micelles. Macromolecules 48 (8):2667–2676

Lu J, Bates FS, Lodge TP (2016) Addition of corona block homopolymer retards chain exchange in solutions of block copolymer micelles. Macromolecules 49 (4):1405–1413

Luo G, Zhang Q, Castillo ARD, Urban V, O'Neill H (2009) Characterization of sol−gel-encapsulated proteins using small-angle neutron scattering. ACS Appl Mater Interfaces 1(10):2262–2268

Lutkenhaus JL, Hammond PT (2007) Electrochemically enabled polyelectrolyte multilayer devices: from fuel cells to sensors. Soft Matter 3(7):804–816

Lvov Y, Decher G, Moehwald H (1993) Assembly, structural characterization, and thermal behavior of layer-by-layer deposited ultrathin films of poly(vinyl sulfate) and poly(allylamine). Langmuir 9 (2):481–486

Mandal SS, Bhaduri S, Amenitsch H, Bhattacharyya AJ (2012) Synchrotron small-angle x-ray scattering studies of hemoglobin nonaggregation confined inside polymer capsules. J Phys Chem B 116(32):9604–9610

Mariani G, Moldenhauer D, Schweins R, Grohn F (2016) Elucidating electrostatic self-assembly: molecular parameters as key to thermodynamics and nanoparticle shape. J Am Chem Soc 138(4):1280–1293

Matsusaki M, Akashi M (2009) Functional multilayered capsules for targeting and local drug delivery. Expert Opin Drug Deliv 6(11):1207–1217

Mattingly SJ, O'Toole MG, James KT, Clark GJ, Nantz MH (2015) Magnetic nanoparticle-supported lipid bilayers for drug delivery. Langmuir 31 (11):3326–3332

Mjahed H, Porcel C, Senger B, Chassepot A, Netter P, Gillet P, Decher G, Voegel J-C, Schaaf P, Benkirane-Jessel N, Boulmedais F (2008) Micro-stratified architectures based on successive stacking of alginate gel layers and poly(l-lysine)-hyaluronic acid multilayer films aimed at tissue engineering. Soft Matter 4 (7):1422–1429

Naruse K, Eguchi K, Akiba I, Sakurai K, Masunaga H, Ogawa H, Fossey JS (2009) Flexibility and cross-sectional structure of an anionic dual-surfactant wormlike micelle explored with small-angle x-ray scattering coupled with contrast variation technique. J Phys Chem B 113(30):10222–10229

Nguyen T-H, Hanley T, Porter CJH, Boyd BJ (2011) Nanostructured liquid crystalline particles provide long duration sustained-release effect for a poorly water soluble drug after oral administration. J Control Release 153(2):180–186

Nunes SP, Car A (2013) From charge-mosaic to micelle self-assembly: block copolymer membranes in the last 40 years. Ind Eng Chem Res 52(3):993–1003

Patterson JP, Kelley EG, Murphy RP, Moughton AO, Robin M, Lu A, Colombani O, Chassenieux C, Cheung D, Sullivan MO, Epps TH 3rd, O'Reilly RK (2013) Structural characterization of amphiphilic homopolymer micelles using light scattering, SANS, and cryo-TEM. Macromolecules 46(15):6319–6325

Paul A, Vicent MJ, Duncan R (2007) Using small-angle neutron scattering to study the solution conformation of N-(2-hydroxypropyl)methacrylamide copolymer−doxorubicin conjugates. Biomacromolecules 8(5):1573–1579

Pomposo JA, Perez-Baena I, Lo Verso F, Moreno AJ, Arbe A, Colmenero J (2014) How far are single-chain polymer nanoparticles in solution from the globular state? ACS Macro Lett 3(8):767–772

Remant Bahadur KC, Thapa B, Xu P (2012) pH and redox dual responsive nanoparticle for nuclear targeted drug delivery. Mol Pharm 9(9):2719–2729

Richter AG, Dergunov SA, Ganus B, Thomas Z, Pingali SV, Urban V, Liu Y, Porcar L, Pinkhassik E (2011) Scattering studies of hydrophobic monomers in liposomal bilayers: an expanding shell model of monomer distribution. Langmuir 27(7):3792–3797

Riley T, Heald CR, Stolnik S, Garnett MC, Illum L, Davis SS, King SM, Heenan RK, Purkiss SC, Barlow RJ, Gellert PR, Washington C (2003) Core−shell structure of PLA−PEG nanoparticles used for drug delivery. Langmuir 19(20):8428–8435

Rissanen S, Kumorek M, Martinez-Seara H, Li Y-C, Jamróz D, Bunker A, Nowakowska M, Vattulainen I, Kepczynski M, Róg T (2014) Effect of PEGylation on drug entry into lipid bilayer. J Phys Chem B 118 (1):144–151

Rube A, Hause G, Mader K, Kohlbrecher J (2005) Core-shell structure of miglyol/poly(D,L-lactide)/poloxamer nanocapsules studied by small-angle neutron scattering. J Control Release 107(2):244–252

Rubner MF, Cohen RE. Layer-by-layer processed multilayers: challenges and opportunities. In: Decher G, Schlenoff JB (eds) Multilayer thin films: sequential assembly of nanocomposite materials. 2nd edn. Wiley-VCH Verlag GmbH & Co. KGaA, Weinheim

Sakamoto S, Sanada Y, Sakashita M, Nishina K, Nakai K, Yusa S-I, Sakurai K (2014) Chain-length dependence of polyion complex architecture bearing phosphobetaine block explored using SAXS and FFF-MALS. Polym J 46(9):617–622

Salentinig S, Tangso KJ, Hawley A, Boyd BJ (2014) pH-driven colloidal transformations based on the vasoactive drug nicergoline. Langmuir 30(49):14776–14781

Salva R, Le Meins J-F, Sandre O, Brûlet A, Schmutz M, Guenoun P, Lecommandoux S (2013) Polymersome shape transformation at the nanoscale. ACS Nano 7 (10):9298–9311

Sanada Y, Akiba I, Sakurai K, Shiraishi K, Yokoyama M, Mylonas E, Ohta N, Yagi N, Shinohara Y, Amemiya Y (2013) Hydrophobic molecules infiltrating into the poly(ethylene glycol) domain of the core/shell interface of a polymeric micelle: evidence obtained with anomalous small-angle x-ray scattering. J Am Chem Soc 135(7):2574–2582

Sauer M, Meier W (2004) Polymer nanocontainers for drug delivery. In: Carrier-based drug delivery, vol 879. American Chemical Society, pp 224–237

Schnablegger H, Singh Y (2013) The SAXS guide, 3rd edn. Anton Paar GmbH, Austria

Shutava TG, Lvov YM (2006) Nano-engineered microcapsules of tannic acid and chitosan for protein encapsulation. J Nanosci Nanotechnol 6 (6):1655–1661

Shutova TG, Agabekov VE, Lvov YM (2007) Reaction of radical cations with multilayers of tannic acid and polyelectrolytes. Russ J Gen Chem 77(9):1494–1501

Skirtach AG, Yashchenok AM, Mohwald H (2011) Encapsulation, release and applications of LbL polyelectrolyte multilayer capsules. Chem Commun 47 (48):12736–12746

Smith GN, Alexander S, Brown P, Gillespie DAJ, Grillo I, Heenan RK, James C, Kemp R, Rogers SE, Eastoe J (2014) Interaction between surfactants and colloidal latexes in nonpolar solvents studied using contrast-variation small-angle neutron scattering. Langmuir 30(12):3422–3431

Srinivas G, Mohan RV, Kelkar AD (2013) Polymer micelle assisted transport and delivery of model hydrophilic components inside a biological lipid vesicle: a coarse-grain simulation study. J Phys Chem B 117(40):12095–12104

Sukhorukov GB, Möhwald H (2007) Multifunctional cargo systems for biotechnology. Trends Biotechnol 25(3):93–98

Tang Z, Wang Y, Podsiadlo P, Kotov NA (2006) Biomedical applications of layer-by-layer assembly: from biomimetics to tissue engineering. Adv Mater 18 (24):3203–3224

Tong W, Gao C (2008) Multilayer microcapsules with tailored structures for bio-related applications. J Mater Chem 18(32):3799–3812

Urbina MC, Zinoveva S, Miller T, Sabliov CM, Monroe WT, Kumar CSSR (2008) Investigation of magnetic nanoparticle−polymer composites for multiple-controlled drug delivery. J Phys Chem C 112 (30):11102–11108

Veronese FM, Mero A (2012) The impact of PEGylation on biological therapies. BioDrugs 22(5):315–329

Vicent MJ, Greco F, Nicholson RI, Paul A, Griffiths PC, Duncan R (2005) Polymer therapeutics designed for a combination therapy of hormone-dependent cancer. Angew Chem Int Ed 44(26):4061–4066

Vogtt K, Jeworrek C, Garamus VM, Winter R (2010) Microdomains in lipid vesicles: structure and distribution assessed by small-angle neutron scattering. J Phys Chem B 114(16):5643–5648

Von White G, Mohammed FS, Kitchens CL (2011) Small-angle neutron scattering investigation of gold nanoparticle clustering and ligand structure under antisolvent conditions. J Phys Chem C 115 (38):18397–18405

Wang Y, Angelatos AS, Caruso F (2008) Template synthesis of nanostructured materials *via* layer-by-layer assembly. Chem Mater 20(3):848–858

Xue B, Kozlovskaya V, Liu F, Chen J, Williams JF, Campos-Gomez J, Saeed M, Kharlampieva E (2015) Intracellular degradable hydrogel cubes and spheres for anti-cancer drug delivery. ACS Appl Mater Interfaces 7(24):13633–13644

Yang B, Lowe JP, Schweins R, Edler KJ (2015a) Small angle neutron scattering studies on the internal structure of poly(lactide-co-glycolide)-block-poly(ethylene glycol) nanoparticles as drug delivery vehicles. Biomacromolecules 16(2):457–464

Yang W, Lu J, Gilbert EP, Knott R, He L, Cheng W (2015b) Probing soft corona structures of DNA-capped nanoparticles by small angle neutron scattering. J Phys Chem C 119(32):18773–18778

Yin P, Wu B, Mamontov E, Daemen LL, Cheng Y, Li T, Seifert S, Hong K, Bonnesen PV, Keum JK, Ramirez-Cuesta AJ (2016) X-ray and neutron scattering study of the formation of core-shell-type polyoxometalates. J Am Chem Soc 138:2638–2643

Yokoyama M, Okano T, Sakurai Y, Suwa S, Kataoka K (1996) Introduction of cisplatin into polymeric micelle. J Control Release 39(2):351–356

Zavgorodnya O, Kozlovskaya V, Kharlampieva E (2015) Nanostructured highly-swollen hydrogels: complexation with amino acids through copper (II) ions. Polymer 74:94–107

Zeno WF, Hilt S, Aravagiri KK, Risbud SH, Voss JC, Parikh AN, Longo ML (2014) Analysis of lipid phase behavior and protein conformational changes in nanolipoprotein particles upon entrapment in sol–gel-derived silica. Langmuir 30(32):9780–9788

Zhu Q, Harris MT, Taylor LS (2011) Time-resolved SAXS/WAXS study of the phase behavior and microstructural evolution of drug/PEG solid dispersions. Mol Pharm 8(3):932–939